Catalytic tar removal using TiO$_2$/NiWO$_4$-Ni$_5$TiO$_7$ films

Jing Xu[a], Philip Holthaus[b], Nianjun Yang[a,*], Siyu Jiang[c], Alwin Heupel[b], Holger Schönherr[c], Bing Yang[d], Wolfgang Krumm[b], Xin Jiang[a,*]

[a] *Institute of Materials Engineering, University of Siegen, 57076, Siegen, Germany*
[b] *Institute for Energy and Environmental Process Engineering, University of Siegen, 57076, Siegen, Germany*
[c] *Physical Chemistry I, Department of Chemistry and Biology & Research Center of Micro and Nanochemistry and Engineering (Cμ), University of Siegen, 57076, Siegen, Germany*
[d] *Shenyang National Laboratory for Materials Science, Institute of Metal Research (IMR), Chinese Academy of Sciences (CAS), No.72 Wenhua Road, Shenyang, 110016, China*

ARTICLE INFO

ABSTRACT

One-dimensional nickel catalysts are more promising than nickel powders for catalytic tar removal from biomass gasification, originating from their unique morphologies and higher specific surfaces. Herein, we demonstrate the application of a Ti supported multilayer system, namely a TiO$_2$/NiWO$_4$-Ni$_5$TiO$_7$ film, for catalytic tar removal. This film is synthesized *via* plasma electrolytic oxidation (PEO) combined with subsequently impregnation and annealing. The surface morphology and the size of as-synthesized Ni$_5$TiO$_7$ nanowires are determined mainly by used electrolytes during PEO processes. For catalytic tar removal, a fixed bed reactor is utilized and naphthalene is chosen as a model tar. This TiO$_2$/NiWO$_4$-Ni$_5$TiO$_7$ film exhibits higher efficiency than thermal cracking as well as long-term stability towards catalytic steam reformation of naphthalene. A naphthalene conversion rate of 63% is achieved at 800 °C with a short residence time of 0.34 s and a high tar load of 75 g m$_N^{-3}$. Such a TiO$_2$-NiWO$_4$/Ni$_5$TiO$_7$ film is thus promising for future tar removal from biomass gasification in the industry.

1. Introduction

Fossil fuel is the major energy source for modern society. Due to its limited reserve, huge efforts have been devoted to developing renewable energy. Technologies such as solar and wind are unpredictable, resulting in variable and intermittent energy supply. Biomass, as one of the most important alternative energy resources, has thus attracted significant attention, mainly due to the low cost of raw materials and its stable energy supply. Through gasification, biomass converts to a gas mixture consisting of mainly hydrogen (H$_2$) and carbon monoxide (CO), which has been widely used as a gaseous fuel for heat or power generation. It can also be utilized as synthetic gas (namely syngas) for the production of liquid fuels and synthetic oils *via* the Fischer-Tropsch process (e.g., its conversion into methane or methanol) [1]. Unfortunately, such a gas mixture generated from biomass gasification usually contains a high amount of tars. The formation of such a complex mixture containing condensable organic compounds (or tars) is undesirable since it leads to serious equipment corrosion. Hence, it is urgent to find solutions to eliminate tar (namely tar removal) for successful and efficient production of syngas from biomass.

For tar removal, one of the most promising methods is to catalytically reform tars into gaseous components at a relatively low temperature (600–900 °C). A lot of materials (e.g., Rh-, Pd-, Ru-, Ni-contained compounds, etc.) have been proven to be high-performance catalysts for tar removal. Among them, Ni-based catalysts have been more widely used due to their low cost and high availability. A wide variety of nickel catalysts are even commercially available (e.g., ICI46-1. UCG90-C, Z409, and RZ409) [2]. However, these nickel catalysts are always fast deactivated. This is due to the low resistance against sulfur poisoning and coking [3].

For efficient tar removal, the surface of catalysts needs to be active and highly exposed to tars. Production of nanometer-sized catalysts or related nanostructures is thus the most general approach. For example, synthesized metal oxide nanomaterials (e.g., nano TiO$_2$ [4], NiO [5,6], MgO [7], Fe$_2$O$_3$ [8], CaO [9,10]) by means of different approaches have been proved to be efficient catalysts for catalytic tar removal. These nanometer-sized catalysts usually adhere on porous ceramic supporters (e.g., Al$_2$O$_3$, Olivine) *via* traditional processes such as sol-gel, impregnation, and hydrothermal methods. However, the adhesion force between the catalysts and supporter is low and thus the stability of these

hybrid catalysts is poor. Moreover, most nanoparticles are often formed only in a relatively thin layer and the overall specific surface areas of the catalysts are thus not too big. Furthermore, most of the supporters are brittle and the transportation of these hybrid catalysts in a large scale is actually impossible in most cases, inevitably restricting industrial their applications for catalytic tar removal. Therefore, the synthesis of integrated supporter with nanostructured catalysts for tar removal is of great importance.

Recently, needle-like Ni_5TiO_7 is shown as a new but efficient catalyst for tar removal. Owing to its high surface area and unique three-dimensional geometry, needle-like Ni_5TiO_7 exhibits two-order higher catalytic ability for catalytic tar removal than commercial catalyst (G117) [11]. Here, needle-like Ni_5TiO_7 was synthesized *via* a flux method, followed by annealing treatment at a high temperature (1200–1300 °C) [12]. One additional process was further applied to transfer Ni_5TiO_7 to a supporter. Later, a three-step process was developed to synthesize Ni_5TiO_7 nanowires, including a plasma electrolytic oxidation (PEO) treatment, impregnation, and an annealing process [13]. Through variation of concentration of the impregnation solution, the morphology and structure of Ni_5TiO_7 nanowires have been tailored [13]. The PEO process has been found to be the key to control the growth of Ni_5TiO_7 nanowires, because PEO contributes to the initial nucleation of Ni_5TiO_7 at high discharging energy of PEO. However, the influence of applied experimental conditions during PEO processes on the growth of Ni_5TiO_7 is still ambiguous.

Different from those reported, in this work a $TiO_2/NiWO_4$-Ni_5TiO_7 film is synthesized directly on a Ti substrate. Since such a composite film features a large surface area and introduces additional functional materials of TiO_2 and $NiWO_4$, it is expected to be more stable than Ni_5TiO_7 nanowires and eventually more efficient for catalytic tar removal. Note that, tar from biomass gasification is actually a complicated mixture of aromatic hydrocarbons. Here, a simplified model tar, naphthalene (a two-ring aromatic hydrocarbon) is selected. This is because in tar mixtures it is highly stable and the most difficult component to be decomposed [14,15,16]. Moreover, its concentration in the tar from biomass gasification is high. For example, a typical tar composition from fluidised bed biomass gasification is known to contain 10 to 30% naphthalene [17,18]. Prior to catalytic tar removal, the conditions for the synthesis of $TiO_2/NiWO_4$-Ni_5TiO_7 films are first optimized, including used electrolytes, applied voltage and time during PEO process. The growth mechanism of a $TiO_2/NiWO_4$-Ni_5TiO_7 film grown under different conditions is then discussed. After that, a $TiO_2/NiWO_4$-Ni_5TiO_7 film grown under the optimized conditions is employed for catalytic tar removal and the catalytic performance (e.g., efficiency and long-term stability etc.) is detailed.

2. Experimental

2.1. Materials and specimen preparation

The $TiO_2/NiWO_4$-Ni_5TiO_7 films were synthesized using a two-electrode PEO system. A titanium wire with a diameter of 2 mm (Alfa Aesar, 99.7% purity) was used as the anode. During the PEO process, it was positioned in the center of a cylindrical stainless-steel cathode which was fixed in an electrolytic bath. The PEO treatment was carried out in a double-wall glass cell. The temperature in this cell was controlled precisely with an external thermostat. The PEO process was conducted in five different electrolytes **(Table S1)**, which are shorted as BNi, BNiP, BNiPW, BNiPCa and BNiPWCa throughout the text. The electrolytes were continuously stirred with a magnetic stir bar spanning at a constant rate of 350 rev min^{-1}. A DC power supply (EA-PSI 8720. Conrad Electronics) was used. For all PEO treatments, a constant voltage of 280 V and a reaction time of 15 min were applied. To prevent the device from breakdown, an initial current of 1 A was set. The curves of instantaneous voltage transients were recorded using a LabView program with an interval of 0.1 s. During the PEO process, the electrolyte was

cooled below 20 °C by the circulation of ethylene glycol solution (40 vol %) inside the double-wall glass cell. After the PEO process, the sample was impregnated in 0.1 M $Ni(NO_3)_2$ for 1 h and subsequently annealed at 950 °C for 1 h with a heating and cool rate of 5 °C min^{-1}.

2.2. Characterization

The pH values and conductivities of used electrolytes were measured with a pH-meter and a Zetasizer Nano series (Malvern, UK), respectively. A field emission scanning electron microscope (FE-SEM, Zeiss ultra55, Germany) was used to investigate the morphology of treated surfaces and synthesized samples. An energy-dispersive X-ray spectrometer (EDX) was utilized to identify the chemical composition of these samples. Their phases were identified with X-ray diffraction (XRD), operating at 40 mA and 45 kV. The CuK radiation was used as X-ray source over a 2θ range from 20 to 80° with a step size of 0.01° and a time of 60.00 s pro step. A SSX-100 S-probe photoelectron spectrometer (XPS, Surfaces Science Instruments, Mountain View, USA) with Al Kα radiation of 200 W was utilized to characterize chemical states of these samples. Their XPS survey spectra were measured with 1.0 eV energy resolution from 0 to 1200 eV. The high-resolution spectra were measured with the pass energy of 20 eV and energy resolution of 0.1 eV. The analysis of XPS data was conducted with a CasaXPS processing software (version 2.3.16 PR 1.6).

2.3. Catalytic performance

The performance of a $TiO_2/NiWO_4$-Ni_5TiO_7 film towards catalytic tar removal/conversion was tested in a lab-scale fixed bed reactor, which is schematically shown in **Fig. S1**. The tests were carried out in an electrically heated tubular reactor with an inner diameter of 43 mm. The bulk volume of as-prepared catalysts was 29 cm^3. The mixture of gaseous nitrogen, naphthalene, and steam flew through a packed bed of ceramic spheres to homogenize the gas flow before reaching the catalyst. The composition or the contents of gas products (e.g., CO, H_2, CO_2, CH_4 and O_2) were determined *via* an online gas analyser. Tar sampling and measurements were performed according to DIN CEN/TS 15439:2006. The performance of a $TiO_2/NiWO_4$-Ni_5TiO_7 film for catalytic tar removal was investigated at varied temperatures, residence times (τ) and steam-to-carbon ratios (S/C), and gas hourly space velocities (GHSV).

The value of τ (the ratio of the free volume of the catalysts bed) was estimated using Eq. (1)

$$\tau = \frac{V_K * \varepsilon}{\dot{V}_G} \tag{1}$$

where ε is the porosity of the bed, V_k is the bulk volume, and $\dot{V}_G$ is the feed-gas-flow. While ε was estimated according to Eq. (2)

$$\varepsilon = 1 - \frac{m_K}{\rho_K * V_K} \tag{2}$$

where m_K, ρ_K, and V_K is the density, the weight, and the volume of the catalyst, respectively. For such calculations, non-catalytic thermal decomposition in an empty reactor set-up was conducted under the same boundary conditions.

The values of S/C was calculated based on Eq. (3)

$$S/C = \frac{\frac{m_{H_2O}}{M_{H_2O}}}{\frac{n_C * m_{Tar}}{M_{Tar}}} \tag{3}$$

where m_{H_2O} is the weight of the injected water, M_{H_2O} is the molar mass of water, n_C is the amount of carbon, m_{Tar} is the mass of the injected tar, and M_{Tar} is the molar mass of the injected tar. During the estimation of S/C values, the reactor geometry and the process boundaries (minimum and maximum volume flow and catalysts bed height) were considered.

Based on applied values of τ and S/C for similar tar removal

[14,19,20], the following values were selected in our catalytic systems. The first series of experiments of tar removal was carried out with a τ of 0.25 s and a S/C ratio of 2.2. The tar load in relation to nitrogen feed was varried between 75 g mN^{-3} and 114 g mN^{-3}. The value of GHSV was about 9000 h^{-1}. The reaction temperature was 700, 750, 800, or 850 °C. The applied reaction time was 1 h. Besides this series of experiments, the reaction at 800 °C was also carried out with an increased τ (e.g., 0.34 s) and a reduced GHSV (e.g., 6660 h^{-1}). In the second series of experiments, the S/C ratio was increased up to 4.6. Other conditions were changed to: a reaction temperature of 800 °C, a τ value of 0.34 s, a GHSV value of 6700 h^{-1}, and a tar load speed of 80 g m_N^{-3}. An additional test at 850 °C was performed with a S/C ratio of 4, a similar tar load but a reduced τ of 0.25 s. For the long-term test of $TiO_2/NiWO_4$-Ni_5TiO_7 towards catalytic tar conversion, the applied conditions were: a reaction temperature of 800 °C, a τ of 0.25 s, a S/C ratio of 2.2, a tar load of 75 g m_N^{-3}, and a GSHV value of 9000 h^{-1}.

3. Result and discussion

3.1. Catalyst synthesis and characterization

To synthesize the catalyst (namely the $TiO_2/NiWO_4$-Ni_5TiO_7 film), the used electrolyte must have suitable pH value as well as high electrical conductivity. The influence of chemical compositions of used electrolytes on their properties (e.g., pH values and conductivities) was then investigated. As shown in Fig. 1a, all five electrolytes are slightly alkalized since all pH values are above 7. These electrolytes are actually suspensions due to the formation of $Ni(OH)_2$ and $Ca(OH)_2$ precipitations under alkaline conditions. The highest pH value (8.2) is found for the BNiPW electrolyte. The addition of $Ca(Ac)_2$ into BNiPW reduces its pH value. On the other hand, the conductivity of the BNi electrolyte rises from 8.29 to 14.37 mS cm^{-1} after introducing phosphate ions. The addition of extra tungstate ions (namely the ionized soluble WO_4^{2-}) increases the conductivity of the BNiP electrolyte further up to 17.37 mS cm^{-1}. The BNiPWCa electrolyte exhibits the highest conductivity with a value of 18.03 mS cm^{-1}. This is probably due to the ionization of the additives in the suspension. Therefore, the addition of these chemicals does not affect much the pH values of the electrolytes, but does change dramatically the conductivities of the electrolytes.

It is known that the nucleation of Ni_5TiO_7 nanowires requires a high energy discharge during the PEO process [13]. The discharging phenomenon appears only when the applied voltage exceeds a certain threshold (e.g., breakdown voltage). In other words, a high voltage is necessary during PEO processes. The voltage variation in above-mentioned electrolytes was then recorded as a function of reaction time. Fig. 1b shows the representative voltage-time curves recorded within the initial 200 s in these electrolytes. As expected, such voltage response

is highly sensitive to environmental conditions (e.g., electrolyte composition, solution temperature, etc.). For example, the voltage starts to increase linearly and rapidly within a time frame of 10 s in all electrolytes, but different trends are noticed after this initial stage. The voltage variation in the BNi electrolyte decreases progressively from 172 to 116 V. The gradual reduction of voltage indicates an insufficient ionic current and lower passivation ability since only the ionic current contributes to the voltage evolution at the initial stage [21]. In short, the breakdown voltage in the BNi electrolyte cannot be reached and the initial barrier layer cannot be formed. On the contrary, the voltage response in other four electrolytes containing phosphate ions is varied as a function of the PEO time in a quite similar way. This is because the addition of phosphate ions provides more amounts of Na^{2+} and PO_4^{2-} ions. After about 10 s (or the initial stage of a PEO process), the total current is already composed of both ionic and electronic currents [22]. This relatively high current maintains the applied voltage and exceeds to the breakdown value. The voltage rises continuously before reaching a plateau (about 280 V). In these electrolytes, the required transient times are different. To further clarify such a difference, the breakdown voltage, extracted from the first turning point of each voltage response curve [21], is compared. It follows the sequence of BNiPW (141 V) < BNiP (185 V) < BNiPWCa (188 V) < BNiPCa (192 V). In short, the addition of Na_2WO_4 decreases the value of breakdown voltage, while Ca $(Ac)_2$ does an opposite effect.

The colors of synthesized films using the PEO process were also checked. As shown in Fig. 2a, all samples have different colors. Inhomogeneous colour distribution is observed (even by bare eyes) for the film synthesized in the BNi electrolyte, indication of a failed process. The film synthesized in the PBNi electrolyte exhibits a homogenous white colour, originating from the formed TiO_2 layer during PEO treatment. The samples synthesized in the electrolytes of PBNiW and PBNiCa show a light yellow and dark yellow colour, respectively. The light green colour is observed on the sample synthesized in the PBNiWCa electrolyte, implying a partially successful growth process of Ni_5TiO_7 nanowires. This is because the colour of the Ni_5TiO_7 film is known to be green [12]. Once the outer surface is scratched off, a yellow layer is visible at the bottom. In other words, the film synthesized in the PBNiWCa electrolyte actually consists of two layers. These different colors indicate that they have varied compositions as well as different micro-/nano- structures. Subsequently, the used electrolyte is indeed one of key factors to determine the microstructure and morphology of the films fabricated using such a PEO process.

To support further such a statement, the morphology of these films was checked using FE-SEM. Fig. 2b-f show the SEM images of the films obtained in these electrolytes. Their morphology is obviously varied when the composition of the used electrolytes is changed. Spherical agglomerates are observed on the surface of the film synthesized in the
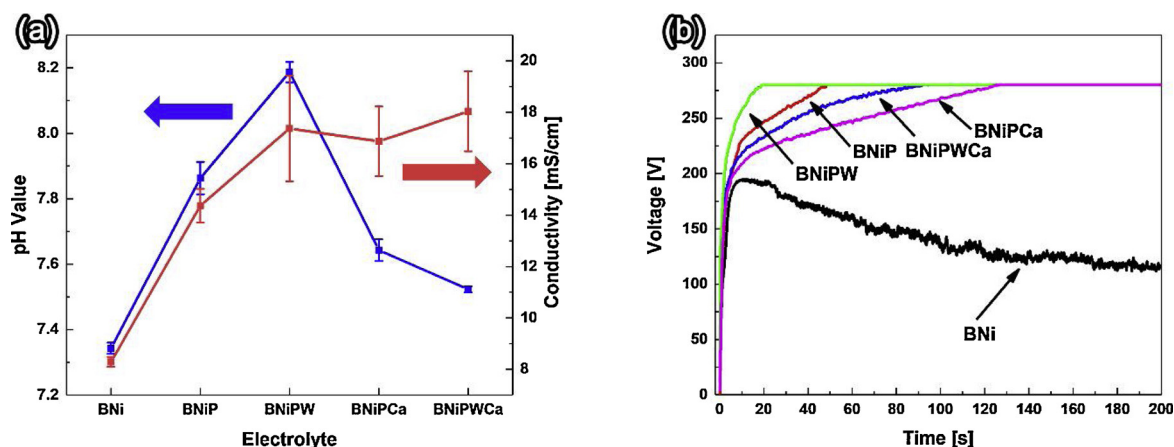

Fig. 1. (a) pH values and conductivities of five electrolytes for the PEO treatment, (b) voltage variation as a function of time during PEO processes in five electrolytes.
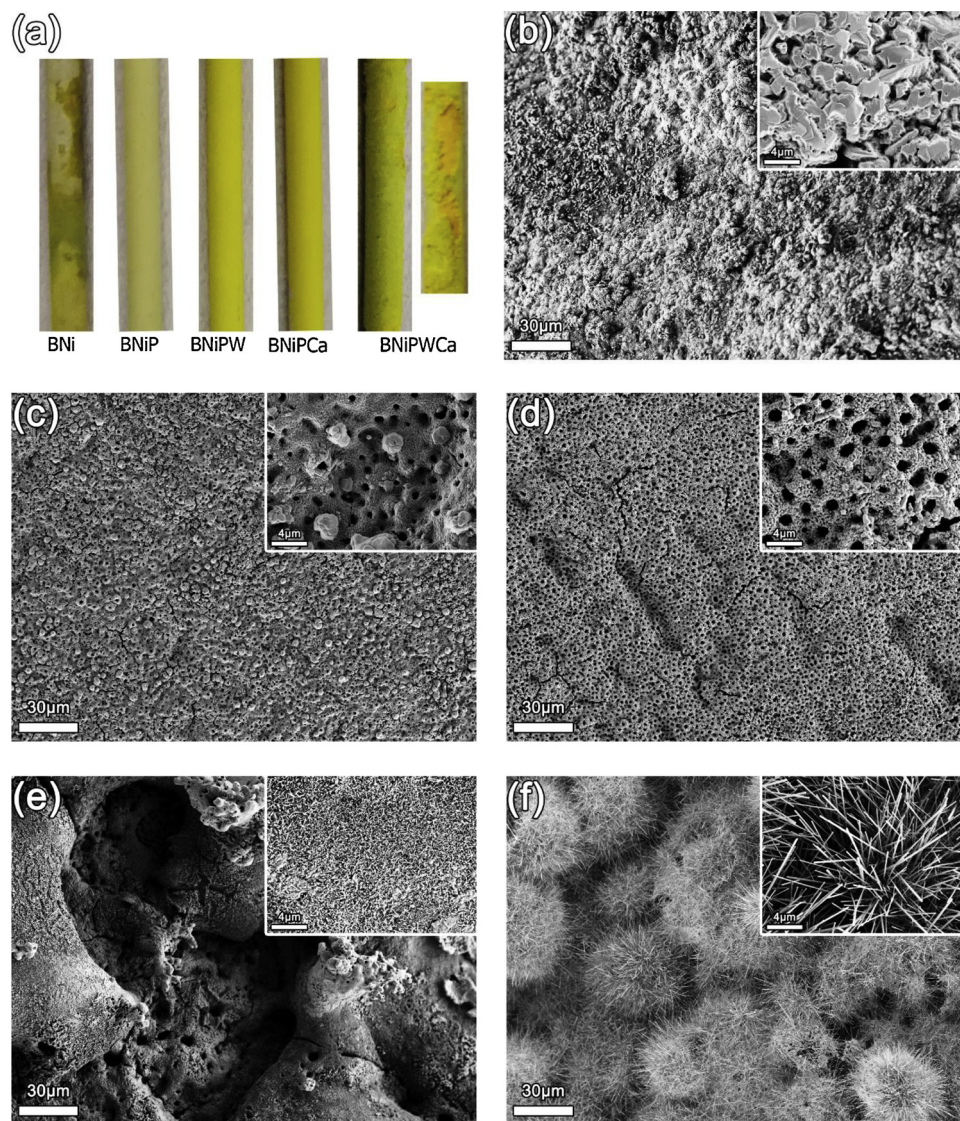
Fig. 2. (a) photographs and (b–f) SEM images of the films synthesized in the electrolytes of BNi (b), BNiP (c), BNiPW (d), BNiPCa (e), and BNiPWCa (f). The insets in (b–f) are related SEM images with high-magnifications.

BNi electrolyte. However, neither the microporous TiO_2 layer nor the Ni_5TiO_7 nanowire is obtained for the film synthesized in the BNi electrolyte. After the addition of phosphate ions (namely in the BNiP electrolyte), the volcano-like porous surface is seen, probably caused by sparking and gas generation at high voltages. The addition of Na_2WO_4 leads to the generation of more cracks, compared to the film synthesized in the BNiP electrolyte, but no Ni_5TiO_7 nanostructures are obtained. For the film synthesized in the electrolytes of BNiP and BNiPW, no significant difference is found in their morphology (**Fig. S2a, S2b**). These spherical agglomerates formed on their surfaces are assumed to be nickel oxide, originating from thermal decomposition [23] of impregnated $Ni(NO_3)_2$ at high temperatures (e.g., 950 °C) for a long time (e.g., 1 h). In contrast, after the introduction of $Ca(Ac)_2$ into the electrolyte, the film synthesized in the BNiPCa electrolyte comprises circular features (**Fig. S2c**). These features are supposed to be formed *via* melting and solidifying $Ca(OH)_2$ precipitation during the micro-arc discharging process at high voltages and high instantaneous surface temperatures. The resultant surface is significantly rough, due to a big porosity and many cracks. In this case, cylindrical-shaped nanowires are clearly seen (Fig. 2e). Moreover, the sizes of as-fabricated nanowires are found to be affected by the used electrolytes. For example, the length of synthesized nanowires in the BNiPCa electrolyte is about

5 μm, while the average length of the nanowires synthesized in the BNiPWCa electrolyte is measured to be 45 μm. Consequently, the addition of tungstate ions promotes dramatically the nanowire growth. However, the film synthesized in the BNiPWCa electrolyte exhibits a highly homogenous surface and is fully covered by dense nanowires. Therefore, the best nanowires (or the best $TiO_2/NiWO_4$-Ni_5TiO_7 films) are synthesized in the BNiPWCa electrolyte.

The growth mechanism of these nanowires in the BNiPWCa electrolyte was further investigated. For such a purpose, two films synthesized in the BNiPWCa electrolyte were mechanically broken. Namely, one was obtained only after a PEO process, another one was fabricated using a PEO process, followed by subsequent impregnation and thermal treatment. Fig. 3a-c show the cross-section SEM images of these films. A crack-rich surface is seen for the film obtained only after a PEO process (Fig. 3a). Two layers are found: a thin outer layer with a thickness of 2 μm and a thick inner layer with an average thickness of about 21 μm (Fig. 3b). More interestingly, this outer layer is exactly the observed crack-rich surface and located above the porous inner layer. In comparison to the outer layer, the inner layer is much rougher. There are visible pores, probably caused by the bubble release during the PEO process.

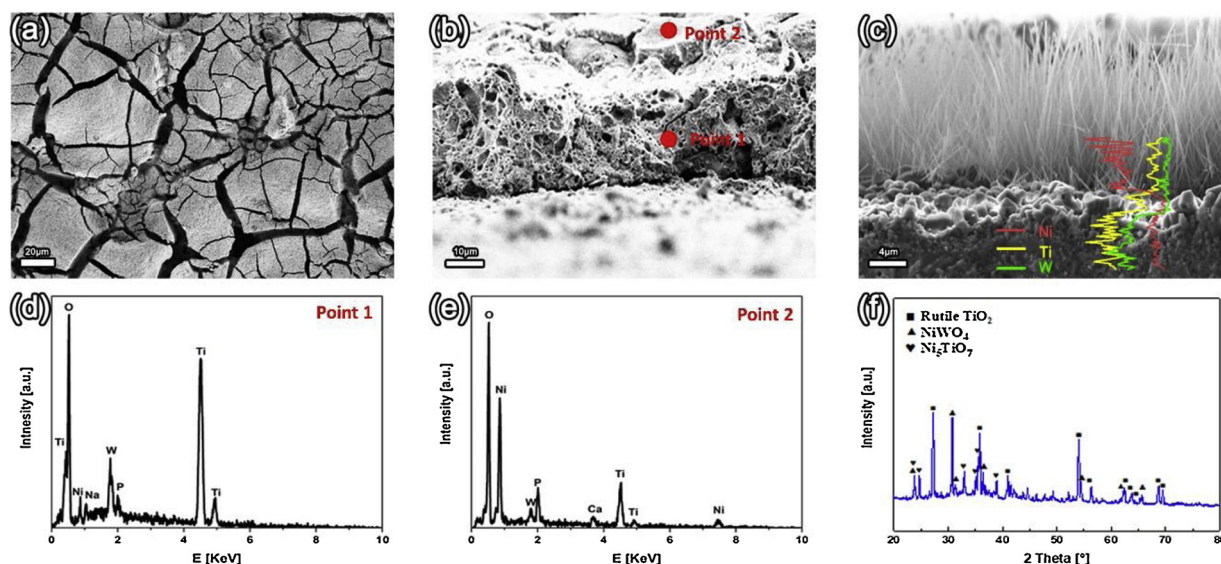The element distribution of the inner and outer layers was also

Fig. 3. SEM images of a Ti substrate after a PEO process in the BNiPWCa electrolyte in the top (a) and side (b) view; (c) SEM cross-sectional image of a $TiO_2/NiWO_4$-Ni_5TiO_7 film. The inset is one EDX line profile. (d,e) EDX line profiles of two points at the inner and outer layer of the film in (b). (f) XRD patterns of the $TiO_2/NiWO_4$-Ni_5TiO_7 film.

examined using EDX composition analysis (Fig. 3d). On the point 1 in the inner layer, main elements of W, Ti, and O are found, while the minor amounts of P, Na, and Ni elements are also detected. It is thus assumed that the inner layer consists mainly of TiO_2 or WO_3 [24]. This is because Na_2WO_4 is soluble and easily ionized to WO_4^{2-} anions. These negatively charged WO_4^{2-} anions rapidly migrate to the anode through electrophoretic field and incorporate into the TiO_2 matrix. In the subsequent annealing process, the WO_3 serves as the precursor for the formation of $NiWO_4$. The EDX analysis of the outer layer (point 2) is shown in Fig. 3e. The peak of Ca element is visible. Considering that Ca $(OH)_2$ and $Ni(OH)_2$ precipitations are the main sources of Ca and Ni elements in the alkaline electrolytes, this thin outer layer is thus believed to be formed by immobilizing these precipitates onto the inner layer. This is based on the fact that the inner layer possesses extremely high micro-roughness and then a number of adhesion sites are provided for $Ni(OH)_2$ precipitation. As a result, a Ni-rich outer layer is formed and served as the Ni precursor for the growth of Ni_5TiO_7 and $NiWO_4$ during the annealing processes.

Fig. 3c shows the SEM image of the film obtained after further annealing the one shown Fig. 3b. Interestingly, the preformed outer layer completely disappears. The elimination of pores from the inner layer is noticed. These changes are the indication of the sintering behavior of Ni_5TiO_7 at high temperatures. The conducted EDX line scans (the inset in Fig. 3c) were then utilized for the examination of elemental variation and distribution along such a film. The content of Ni element in the outer layer is found to be much higher than that in the inner layer. The outer layer (decorated with nanowires) displays a larger amount of the elements of Ni and Ti, but a much lower content of W. In contrast, a much high content of the element of W is found in the inner layer, indicating the $NiWO_4$ mainly exists in the inner layer.

The X-ray diffraction was also used to investigate the phase composition of the film synthesized in the BNiPWCa electrolyte of (Fig. 3f). The TiO_2 rutile phase is clearly detected. Moreover, the XRD patterns for $NiWO_4$ and Ni_5TiO_7 phases are visible. Their dominant peaks are in good agreement with the standard structure data of Ni_5TiO_7 (PDF#31-0917) and $NiWO_4$ (PDF#15-0755) crystals. All these results demonstrate the successful synthesis of the $TiO_2/NiWO_4$-Ni_5TiO_7 film in the BNiPWCa electrolyte.

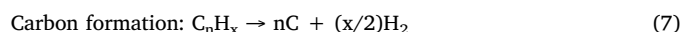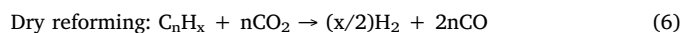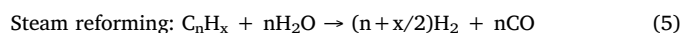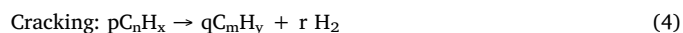To reveal the detailed structures of the $TiO_2/NiWO_4$-Ni_5TiO_7 film fabricated in the BNiPWCa electrolyte, mainly those of the Ni_5TiO_7 nanowires, TEM measurements were conducted. As shown in Fig. 4a,

the lateral size of these nanowires is about 65 nm. From the SAED pattern inserted in Fig. 4, their good crystallinity is confirmed. Their high-resolution TEM presented in Fig. 4b reveals that a lattice distance between two adjacent lattice planes perpendicular to the growth direction is about 0.30 nm, matching well with the D-spacing value of (010) planes of a Ni_5TiO_7 crystal [13].

The chemical composition of these nanowires was further confirmed with XPS measurements. The elements of Ti, O, and Ni are clearly seen (**Fig. S3**). No clean sign of the element of W is found. Note here that this XPS result only reflects the properties of a superficial layer (e.g., with a depth of ~100 nm). In other words, XPS spectrum here only corresponds to the outer layer of Ni_5TiO_7. The high resolution XPS spectra of Ti 2p and Ni 2p were also analyzed (Fig. 4c). For the Ti 2p peak, it is deconvoluted into two distinct peaks with the binding energies of 464.2 eV (2p1/2) and 458.3 eV (2p3/2). Both are attributed to Ti(IV) species in the Ni_5TiO_7, which is actually composed as $5NiO \cdot TiO_2$. For the Ni 2p peak, it is de-convoluted into two satellites and two main lines for Ni 2p3/2 and Ni 2p1/2. Their binding energies are 878.7 and 861.6 eV for the satellites, 873.2 eV for Ni 2p1/2, and 855.5 eV for Ni 2p3/2, respectively [25]. Based on these characterization results, one can conclude that successful synthesis of a $TiO_2/NiWO_4$-Ni_5TiO_7 film has been realized. Such a film features a large surface areas, good crystalline, and highly exposed reaction sites from Ni_5TiO_7 nanowires. Therefore, a $TiO_2/NiWO_4$-Ni_5TiO_7 film is expected to show superior catalytic ability.

3.2. Catalyst performance

This $TiO_2/NiWO_4$-Ni_5TiO_7 film was then applied for catalytic tar conversion. In general, tar removal, conversion, or decomposition occurs in the steps of cracking, steam reformatting, dry reforming, and carbon formation [19,26]. These reactions can be simplified as following:

$$\text{Cracking: } pC_nH_x \rightarrow qC_mH_y + r\,H_2 \qquad (4)$$

$$\text{Steam reforming: } C_nH_x + nH_2O \rightarrow (n+x/2)H_2 + nCO \qquad (5)$$

$$\text{Dry reforming: } C_nH_x + nCO_2 \rightarrow (x/2)H_2 + 2nCO \qquad (6)$$

$$\text{Carbon formation: } C_nH_x \rightarrow nC + (x/2)H_2 \qquad (7)$$
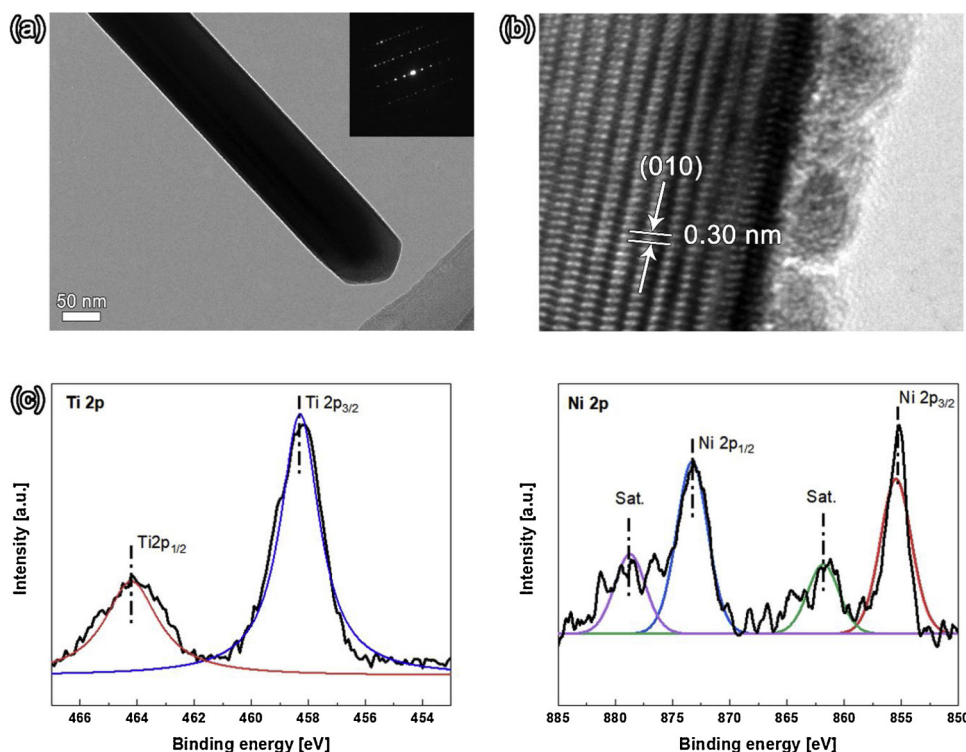
where C_nH_x represents tar and C_mH_y represents hydrocarbons with

Fig. 4. TEM (a) and HRTEM (b) images of a Ni_5TiO_7 nanowire in a $TiO_2/NiWO_4$-Ni_5TiO_7 film as well as their high resolution XPS spectra of Ti 2p (left) and Ni 2p (right) core levels. The inset in image (a) is the SAED pattern. The black lines in (c) are experimental results and the colour lines in (c) are the individually simulated lines.

smaller carbon numbers than C_nH_x. Cracking reactions are supposed to lead to smaller hydrocarbons, and condensation leads to soot [27]. In our case, the catalytic steam reforming of naphthalene, or naphthalene removal can be then expressed in the form of [14]:

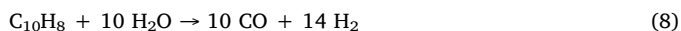$$C_{10}H_8 + 10\ H_2O \rightarrow 10\ CO + 14\ H_2 \qquad (8)$$

Fig. 5a summarizes the variation of the efficiencies of gravimetric tar conversion (namely the mass ratio of removed naphthalene) as a function of the temperatures applied in the first series of experiments. To evaluate the catalytic activity of a $TiO_2/NiWO_4$-Ni_5TiO_7 film under these temperatures, thermal cracking was performed, namely thermal decomposition of naphthalene in the reactor but without adding the catalyst of $TiO_2/NiWO_4$-Ni_5TiO_7. For example, in comparison to catalytic naphthalene removal with the $TiO_2/NiWO_4$-Ni_5TiO_7 catalyst at 800 °C and with a S/C-ratio of 2.2, a much longer τ of 0.64 s and a redued tar laod of 40 g mN^{-3} are required for thermal decomostion of naphthalene to achieve a comparable conversion rate of 45%(item d in Fig. 5a), namely an increase of the τ of approximately 188% with the reduction of naphthalene loading of 47%. At 800 °C, a higher loading of naphthalene (165.9 g m_N^{-3}) and the application of a longer τ (0.525 s) lead to a major drop in conversion or removal rate of naphthalene (26.42%). Similar tendency is observed at other temperatures. At 700 °C, a naphthalene conversion of 25% is achieved with the employment of the $TiO_2/NiWO_4$-Ni_5TiO_7 catalyst. An increase of temperature from 800 to 850 °C leads to much higher activity and an increase of naphthalene conversion of almost 20%. Fig. 5**b** shows the results obtained from the second series of experiments. The gravimetric naphthalene conversion rises with increasing S/C ratio from 45% (S/C = 2.1) to 63% (S/C = 4.1). A further increase of S/C up to 4.6 leads to a decline in naphthalene conversion down to 56%. The $TiO_2/NiWO_4$-Ni_5TiO_7 film clearly favors a maximum naphthalene conversion rate at a higher S/C ratio (e.g., S/C = 4), similar as that reported found when other catalysts (e.g., Ni/Al_2O_3 catalyst) are applied [21]. Such high-performance catalytic performance for tar removal (namely naphthalene conversion into CO and H_2) is similar as that observed on other nanostructured catalysts [4–10]. It is thus believed to originate from the nature of Ni_5TiO_7 (more exactly high catalytic activity of nickel based

catalysts) and highly exposed nickel based catalytic sites that are widely existed on these nanowires [11–13].

The application of a $TiO_2/NiWO_4$-Ni_5TiO_7 film towards long-term catalytic naphthalene conversion was also examined. The obtained results are shown in Fig. 6. After the catalytic conversion for 10 h, a naphthalene conversion efficiency of 45% is achieved, which is 16% higher if compared to that for a fresh catalyst. In other words, the $TiO_2/NiWO_4$-Ni_5TiO_7 catalyst can be activated under these operating conditions. Its ability towards catalytic naphthalene conversion is possible to be improved once a long loading time is applied. Further increase of reaction time (another 3 h for naphthalne conversion) leads to slight improvement of naphthalene conversion (up to 48%) but without coke burn-off. The gas formation (e.g., CO_2 and CO) is negligible during the burn-off process. Applying more hours for tar loading and with coke burn-off did not change the naphthalene conversion (which is remained stable at 45%). During a total reaction time of nearly 16 h, no degradation of this catalyst has been found. Therefore, the $TiO_2/NiWO_4$-Ni_5TiO_7 film owns good resistance to coke formation as the catalyst during naphthalene conversion, leading to its long-term stability towards catalytic naphthalene removal. This is because tungsten compounds (e.g., $NiWO_4$) are known to be excellent coking-resistantpromoters [28].

4. Conclusion

A $TiO_2/NiWO_4$-Ni_5TiO_7 film has been directly synthesized on a Ti substrate using a PEO method combined with subsequent impregnation and annealing processes. This film consists of a Ni_5TiO_7 outer layer and a $TiO_2/NiWO_4$ inner layer, of which morphology and coverage are determined mainly by the used electrolytes. Such a film is successfully utilized for long-term catalytic tar removal (e.g., naphthalene conversion). Moreover, such a catalyst features the flexible nature of Ti metal substrates and high possibility of its large-scale production. To further clarify the catalytic stability of the $TiO_2/NiWO_4$-Ni_5TiO_7 film against coke formation during tar conversion, the systematic experiments need to be conducted using tars containing hydrogen sulfide. The catalysts consisting of more compositions need to be synthesized since they are
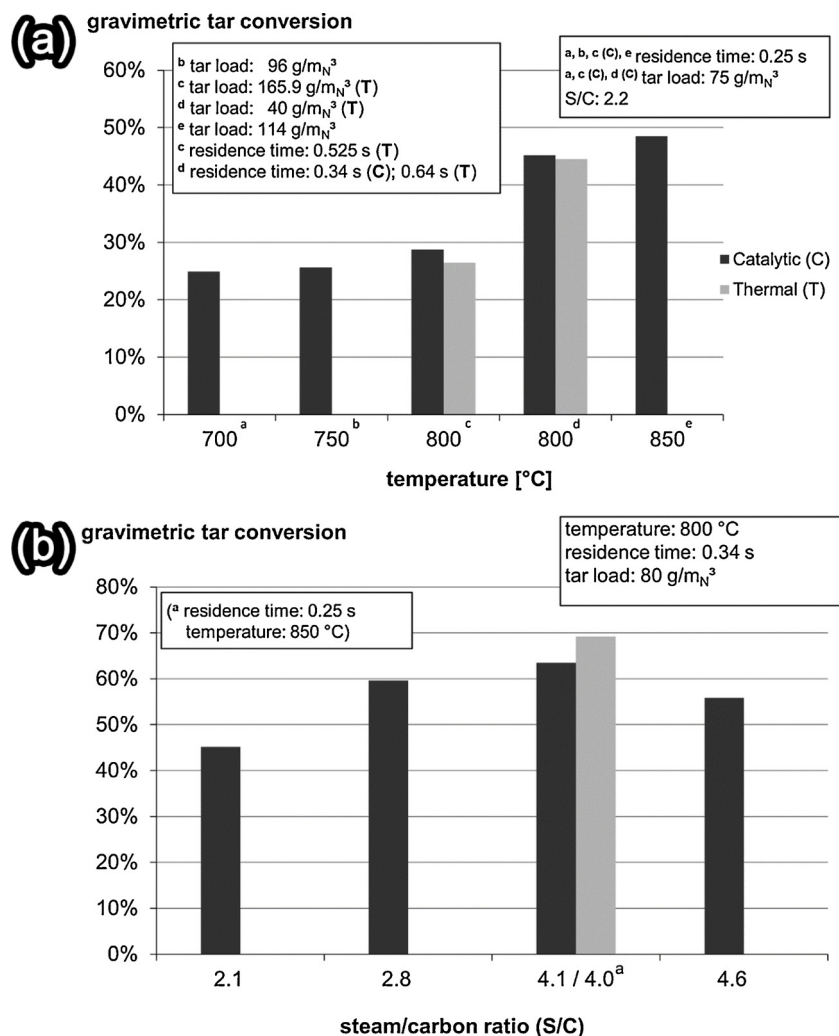
(a) gravimetric tar conversion

[b] tar load: 96 g/m$_N^3$
[c] tar load: 165.9 g/m$_N^3$ (**T**)
[d] tar load: 40 g/m$_N^3$ (**T**)
[e] tar load: 114 g/m$_N^3$
[c] residence time: 0.525 s (**T**)
[d] residence time: 0.34 s (**C**); 0.64 s (**T**)

[a, b, c (C), e] residence time: 0.25 s
[a, c (C), d (C)] tar load: 75 g/m$_N^3$
S/C: 2.2

■ Catalytic (C)
■ Thermal (T)

temperature: 700[a] 750[b] 800[c] 800[d] 850[e]

temperature [°C]

(b) gravimetric tar conversion

temperature: 800 °C
residence time: 0.34 s
tar load: 80 g/m$_N^3$

([a] residence time: 0.25 s
temperature: 850 °C)

steam/carbon ratio: 2.1   2.8   4.1 / 4.0[a]   4.6

steam/carbon ratio (S/C)

Fig. 5. Variation of gravimetric efficiency of naphthalene conversion with (a) applied temperature (from 700 °C to 850 °C) and (b) the S/C ratio (2.1–4.6). In (b), the reaction temperature was 800 °C.
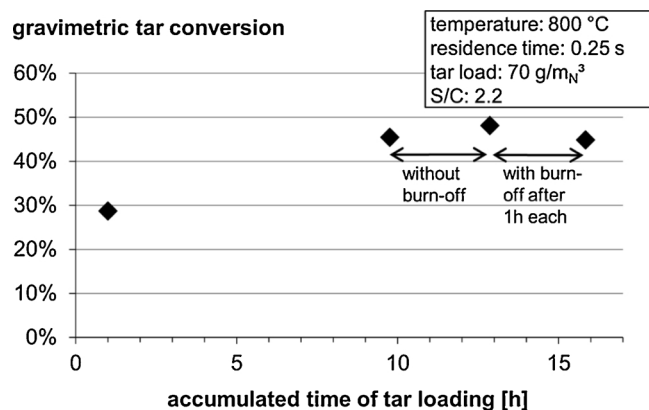

gravimetric tar conversion

temperature: 800 °C
residence time: 0.25 s
tar load: 70 g/m$_N^3$
S/C: 2.2

without burn-off   with burn-off after 1h each

accumulated time of tar loading [h]

Fig. 6. Long-term stability of a $TiO_2/NiWO_4$-Ni_5TiO_7 film for naphthalene conversion at 800 °C with and without burn-off of carbon deposited on the surface of this film.

expected to offer more features, enabling these catalysts to meet the complicated requirements for practical environment protection (e.–g., by means of efficient removal of various pollutants). In summary, the proposed strategy is promising and holds the potential for future tar removal from biomass gasification in the industry.

Acknowledgements

Appendix A. Supplementary data

Supplementary material related to this article can be found, in the online version, at doi:https://doi.org/10.1016/j.apcatb.2019.03.006.

References

[1] M.E. Dry, Catal. Today 71 (2002) 227–241.
[2] Y. Shen, K. Yoshikawa, Renew. Sustain. Energy Rev. 21 (2013) 371–392.
[3] K. Sato, K. Fujimoto, Catal. Commun. 8 (2007) 1697–1701.
[4] Q. Lu, Z.-F. Zhang, C.-Q. Dong, X.-F. Zhu, Energies 3 (2010) 1805.
[5] J. Li, R. Yan, B. Xiao, D.T. Liang, D.H. Lee, Energy Fuels 22 (2008) 16–23.
[6] Y.P. Wang, J.W. Zhu, X.J. Yang, L.D. Lu, X. Wang, Thermochim. Acta 437 (2005) 106–109.
[7] L. Wang, J. Yang, Fuel 86 (2007) 328–333.

[8] F. Shi, M.K. Tse, M.M. Pohl, A. Brückner, S. Zhang, M. Beller, Angew. Chem. Int. Ed. 46 (2007) 8866–8868.

[9] S. Siva, C. Marimuthu, Int. J. Chemtech Res. 7 (2015) 2112–2116.

[10] E. Mosaddegh, A. Hassankhani, Chin. J. Catal. 35 (2014) 351–356.

[11] X. Jiang, L. Zhang, S. Wybornov, T. Staedler, D. Hein, F. Wiedenmann, W. Krumm, V. Rudnev, I. Lukiyanchuk, ACS Appl. Mater. Interfaces 4 (2012) 4062–4066.

[12] S. Fumio, K. Tsutomu, Jpn. J. Appl. Phys. 15 (1976) 1403–1404.

[13] Y. Jiang, B. Liu, L. Yang, B. Yang, X. Liu, L. Liu, C. Weimer, Sci. Rep. 5 (2015) 14330.

[14] S. Vivanpatarakij, D. Rulerk, S. Assabumrungrat, Chem. Eng. Trans., 37 (2014) 205–210.

[15] X. Garcia, K. Hüttinger, Erdöl und Kohle, Erdgas, Petrochemie 43 (1990) 273–281.

[16] R. Coll, J. Salvado, X. Farriol, D. Montane, Fuel Process. Technol. 74 (2001) 19–31.

[17] T.A. Milne, R.J. Evans, N. Abatzaglou, National Renewable Energy Laboratory, Golden, CO (US, 1998 https://www.osti.gov/servlets/purl/3726.

[18] M. Ising, Zur katalytischen Spaltung teerartiger Kohlenwasserstoffe bei der Wirbelschichtvergasung von Biomasse, Fraunhofer IRB Verlage, Oberhausen, Germany, 2002.

[19] C. Li, K. Suzuki, Renew. Sust. Energ. Rev 13 (2009) 594–604.

[20] T. Furusawa, K. Saito, Y. Kori, Y. Miura, M. Sato, N. Suzuki, Fuel 103 (2013) 111–121.

[21] K. Venkateswarlu, N. Rameshbabu, D. Sreeekanth, M. Sandhyarani, A. Bose, V. Muthupandi, S. Subramanian, Electrochim. Acta 105 (2013) 468–480.

[22] L. Chang, J. Alloys. Compd. 468 (2009) 462–465.

[23] W. Brockner, C. Ehrhardt, M. Gjikaj, Thermochim. Acta 456 (2007) 64–68.

[24] R. Hahn, J.M. Macak, P. Schmuki, Electrochem. Commun. 9 (2007) 947–952.

[25] B. Sasi, K. Gopchandran, Nanotechnology 18 (2007) 115613.

[26] L. Devi, K.J. Ptasinski, F.J. Janssen, Biomass Bioenergy 24 (2003) 125–140.

[27] A. Jess, Fuel 75 (1996) 1441–1448.

[28] T. Borowiecki, A. Gołcebiowski, Catal. Lett. 25 (1994) 309–313.